Forecast of Ionospheric TEC Maps Using ConvGRU Deep Learning Over China

Jun Tang, Zhengyu Zhong, Mingfei Ding, Dengpan Yang, and Heng Liu

***Abstract*—In this article, we propose a convolutional gated recurrent unit (ConvGRU) deep learning method to forecast ionospheric total electron content (TEC) over China based on the regional ionospheric maps (RIMs) from 2015 to 2018. First, we use Global Navigation Satellite System observations from the Crustal Movement Observation Network of China to generate the RIMs of China (CRIMs). Second, we use the CRIMs of 2015–2017 as the training set to predict the ionospheric TEC over China in 2018. Finally, comparative experiments are carried out with ConvLSTM, International Reference Ionosphere (IRI), and Center for Orbit Determination in Europe's (CODE's) 1-day predicted Global Ionospheric Map (C1PG) released by CODE. In addition, we add geomagnetic indices (ap, Kp, and Dst) and solar activity index (F10.7) as the training set to analyze the prediction accuracy of the model (using -A if there are no indices, and -B if there are indices). The results illustrate that the prediction accuracy of ConvLSTM-B and ConvGRU-B models are improved on both geomagnetic storm and quiet days, and the improvement is more obvious on geomagnetic storm days. Furthermore, the root mean square error (RMSE) of the ConvGRU-B model decreases by 28%, 22.4%, and 5.9% compared to that of the ConvGRU-A, IRI-2016, and ConvLSTM-B models during geomagnetic storm days, respectively. For the prediction accuracy of a certain grid point, the RMSE of the ConvGRU-B model decreases by 23%, 32.6%, and 19.3% during geomagnetic quiet days and 24.4%, 30.6%, and 15.7% during geomagnetic storm days compared to that of the ConvGRU-A, IRI-2016, and ConvLSTM-B models, respectively. For the forecast accuracy of TEC in different seasons, the performance of the ConvGRU-B model is also better than that of the ConvLSTM-B model in 2018. These results show that the ConvGRU-B model has competitive performance in RIMs prediction over China during the geomagnetic quiet and storm days.**

***Index Terms*—Convolutional gated recurrent unit (ConvGRU), deep learning, forecast, ionosphere, total electron content (TEC).**

I. Introduction

THE ionosphere is the upper part of the atmosphere at a distance of about 60 to 1000 km from the Earth. Total electron content (TEC) is an important parameter to characterize the spatial and temporal variability of the ionosphere. There are several studies that considered broadcasting or empirical models for ionospheric TEC forecasting, such as the Klobuchar model [1], [2], International Reference Ionosphere (IRI) model [3], NeQuick model [4], and BDGIM [5]. The prediction accuracy of these models for one-day TEC is less than 70% [6]. Since the establishment of the International Global Navigation Satellite System (GNSS) Service ionospheric working group, many analysis centers such as the Center for Orbit Determination in Europe (CODE), the European Space Agency (ESA), the Jet Propulsion Laboratory (JPL), and the Universitat Politècnica de Catalunya (UPC) in Spanish have provided high-accuracy Global Ionospheric Map (GIM). Also, the CODE, the ESA, and the UPC provide ionospheric prediction products of one day and two days in advance [7], [8]. Monitoring and forecasting of the TEC can provide for the proper operation of real-time navigation, positioning, and communication, as well as reduce the negative impact of the ionosphere on people's production and life. Therefore, it is necessary for us to establish a high-precision ionospheric TEC prediction model.

In recent years, more and more researches have used the deep learning method, which can reflect TEC variations well and has a better fitting effect on nonlinear data, to establish a TEC prediction model [9], [10], [11], [12], [13], [14], [15], [16], [17], [18], [19], [20], [21], [22], [23]. For global TEC forecasting, Lee et al. [11] proposed a TEC forecast model based on a generative adversarial network, and its forecast accuracy was higher than the 1-day forecast product released by CODE. Xiong et al. [14] proposed an encoder–decoder long short-term memory (LSTM) extended neural network method, which showed a strong ability to improve TEC predictions in different geographical locations, seasons, and geomagnetic conditions. Chen et al. [15] combined convolution calculation and LSTM with spectrum analysis, which had a good performance in predicting the global ionospheric TEC from 2015 to 2019. Ren et al. [17] used LSTM with different solar and geomagnetic activity parameters to predict global TEC and found that the prediction accuracy outperformed the conventional mathematical methods under different conditions. Xia et al. [20] established an ED-ConvLSTM model to forecast global ionospheric TEC and compared it with the 1-day forecast model of the Beijing University of Aeronautics and Astronautics (BUAA) and IRI-2016 model. The forecast accuracy was higher than that of BUAA and IRI-2016 models. For regional TEC forecasting, Huang et al. [9] used a genetic algorithm to optimize the traditional BPNN to forecast TEC at four

Manuscript received 23 May 2023; revised 28 October 2023 and 26 December 2023; accepted 31 December 2023. Date of publication 3 January 2024; date of current version 22 January 2024. This work was supported by the National Natural Science Fund of China Grant 42261074. *(Corresponding author: Jun Tang.)*

Jun Tang is with the Faculty of Land Resources Engineering, Kunming University of Science and Technology, Kunming 650093, China, and also with the School of Transportation Engineering, East China Jiaotong University, Nanchang 330013, China (e-mail: townjun@gmail.com).

Zhengyu Zhong, Mingfei Ding, Dengpan Yang, and Heng Liu are with the School of Transportation Engineering, East China Jiaotong University, Nanchang 330013, China (e-mail: 951231272@qq.com; dingmingfei@ecjtu.edu.cn; yangdengpan@ecjtu.edu.cn; hengliu@ecjtu.edu.cn).

Digital Object Identifier 10.1109/JSTARS.2024.3349392

stations in China, and the prediction effect was better than the traditional BPNN model in low and medium solar activity years. The CNN-LSTM combined model established by Ruwali et al. [12] not only retained the time feature extraction capability of the LSTM model but also obtained the spatial feature extraction capability, which had a good forecast effect on the low latitude region of India. Sivakrishna et al. [19] applied a bidirectional LSTM algorithm to predict TEC data over the Indian region and illustrated that the potential of bi-LSTM in time series processing is enhanced by having both forward and backward connections. Liu et al. [23] presented a machine learning method based on principal component analysis and least-square regression to predict TEC over Europe. The above studies have shown that the LSTM model performs well in forecasting ionospheric TEC. The LSTM model effectively improves the problem of gradient explosion and gradient disappearance existing in the traditional recursive neural network when calculating and updating the parameters in the backpropagation.

At present, there are two ways of integrating convolution calculation and LSTM network: CNN-LSTM and ConvLSTM. The former extracts spatial features by stacking CNN layers and then feeds them into the LSTM network. Since the input data of LSTM is 1-D, there are limitations in the prediction of regional TEC. The latter is to replace all the fully connected layers in the LSTM network with convolution calculations, which further strengthens the ability of the model to extract spatial features and is more suitable for regional TEC prediction. The comparative experiments between the ConvLSTM model, CNN-LSTM model, and LSTM are carried out by Gao and Yao [24], which proved that the ConvLSTM model performs the best in TEC forecasting. The GRU model, as an excellent variant of the LSTM model, has a reduced gate structure compared to the LSTM model, which greatly reduces the computational effort of model training and can save a lot of arithmetic power. The model inputs of traditional GRU and LSTM networks are usually 1-D vectors, and the relative position relationships are easily lost when a 2-D TEC matrix is input. In addition, there are fewer studies to establish models for ionospheric TEC forecasting over China based on GNSS observations of the Crustal Movement Observation Network of China (CMONOC) and deep learning methods.

However, there are still some issues with the methods mentioned above. The conventional DCGAN-based approach used in the literature [11] is restricted by the model's complex learning mechanism and training process, which requires more time and memory for training and is more susceptible to problems such as gradient vanishing and pattern collapse. DCGAN is a complex neural network that trains a generator and a discriminator to approximate real prediction results. This learning and training mode requires training an additional subnetwork compared to other time-series forecasting models, resulting in the need for more time and computational resources to fit the time-series data in DCGAN-based forecasting models. In addition, it should be noted that DCGAN and other similar networks may have inherent flaws, such as gradient vanishing and model collapse. Gradient vanishing is a phenomenon that occurs when deep neural networks are trained using error backpropagation. It refers to the fact that the gradient hardly causes any numerical perturbation when propagating backward to the shallow layer, which ultimately leads to slow convergence or convergence failure of the neural network. DCGAN is known to suffer from the problem of gradient vanishing, and interestingly, the better the discriminator is trained, the worse the gradient vanishing of the generator becomes. Pattern collapse is a phenomenon where DCGAN is limited to generating images that are similar to the training data, leading to a lack of diversity in the generated images.

According to the literature [9], regional ionospheric forecasting based on BP neural networks presents several issues. First, BP neural networks are linear input–output networks that can only model data in the temporal dimension and cannot fit data in the spatial dimension well. This limitation is not favorable for regional TEC prediction. Second, fully connected neural networks have more parameters. As the number of parameters increases during neural network training, the model becomes more susceptible to overfitting. This can lead to longer training times and increased space occupation.

The literature suggests that LSTM-like methods, such as those used in [12], [14], [15], [17], and [19], are an improvement over previous methods. However, these methods are not applicable to the task of regional ionospheric TEC prediction due to their 1-D input data. In addition, the traditional LSTM model often uses a fully connected form, which results in more computational parameters, higher computational costs, and longer training time. It is important to note that while CNN-LSTM can input image data, its loose coupling with LSTM increases training costs. ConvLSTM is a more cost-effective solution for handling spatial data compared to CNN-LSTM. This is because ConvLSTM replaces the fully connected layers in traditional LSTM with convolutional layers, reducing training costs. In addition, pruning the internal structure of LSTM can further reduce training costs. This article proposes a deep learning model called convolutional gated recurrent unit (ConvGRU) to achieve faster training.

Compared to the DCGAN model used in the literature [11], ConvGRU requires no separate training of the generator and discriminator to complete the task, making it less susceptible to issues such as gradient disappearance and pattern collapse. In addition, training time has been reduced. Compared to the BP neural network model proposed in the literature [8], [9], ConvGRU can directly process 2-D spatial data by integrating the internal work of CNN. Thanks to the simplification of the ConvGRU structure, it adopts a CNN network instead of the original fully connected network in the fully connected neural network. The current layer of the fully connected neural network is replaced by a CNN network. Compared to the BP neural network model proposed in the literature [9], ConvGRU integrates the CNN internal work to handle 2-D spatial data. The structure of ConvGRU is simplified, and it adopts the CNN network to replace the original fully connected network. In the original fully connected neural network, each neuron in the current layer is connected to every neuron in the previous and later layers. The model's training requires the computation and updating of the weights and biases of each connection, which is a time-consuming process. The training of the model requires the

computation and updating of weights and biases on each connection, which is computationally intensive and time-consuming. The CNN model's convolutional kernel mechanism simplifies the model and shortens training time by only calculating and updating kernel parameters during training. In contrast to the LSTM classes mentioned earlier, ConvGRU can handle spatial 2-D data directly and simplifies the traditional LSTM model significantly. It is much simpler than the LSTM, CNN-LSTM, and GRU models. Like LSTM and GRU models, ConvGRU models also use CNN networks to replace all fully connected networks inside the original model. This allows the model to directly process 2-D data and reduces the time and space complexity of the model. The use of CNN networks in ConvGRU models is a significant improvement over the original model. Compared to ConvLSTM, ConvGRU has a more concise computational formula due to having one less gate and memory cell, resulting in fewer parameters. This reduces training time and improves model time complexity compared to the improved ConvLSTM. Section IV provides a quantitative time complexity analysis of various models. The model is developed and evaluated based on geomagnetic and solar activity indexes, and TEC grid data obtained from modeling with CMONOC observations.

II. Ionospheric TEC Modeling

In this section, we introduce the TEC for prediction model. We use dual-frequency GNSS observation data from the CMONOC stations to construct a high-precision ionospheric model over China. In this study, the TEC is obtained from dual-frequency GNSS observations using the uncombined precise point positioning (UPPP) method [25], [26]. The ionospheric delay estimated by the UPPP method includes the unbiased ionospheric delay and the differential code bias (DCB) from the receiver and satellite [27]. The function can be written as

$$I = I_u + \frac{1}{1-\gamma_2}(\mathrm{DCB}_r - \mathrm{DCB}^s) \tag{1}$$

where I is the estimated ionospheric delay, I_u is the unbiased ionospheric delay, $\gamma_2 = f_1^2/f_2^2$, and DCB_r and DCB^s are the DCB from receiver and satellite, respectively.

Then, a fourth-order spherical harmonic model is applied to construct the vertical TEC (VTEC) model of China. It can be expressed as

$$\mathrm{VTEC}(\beta, s) = \sum_{n=0}^{n_{\max}} \sum_{m=0}^{n} \tilde{P}_{nm}(\sin\beta)\cdot \left(a_{nm}\cos(ms) + b_{nm}\sin(ms)\right) \tag{2}$$

where β denotes the geomagnetic latitude of the ionospheric puncture point, $n_{\max}$ denotes the highest order of the spherical harmonic function expansion, $\tilde{P}_{nm}$ represents the normalized associated Legendre function of order n and degree m, $s = \mathrm{UT} - \lambda - \pi$ represents the daily fixed longitude of the puncture point, λ represents the geomagnetic longitude of the puncture point, UT represents the universal time at the observation time, and a_{nm} and b_{nm} represent the spherical harmonic function model parameter to be solved. The detailed modeling process can be found in [28] and [29]. It has been proved that the regional ionospheric model based on this method has high accuracy [30].

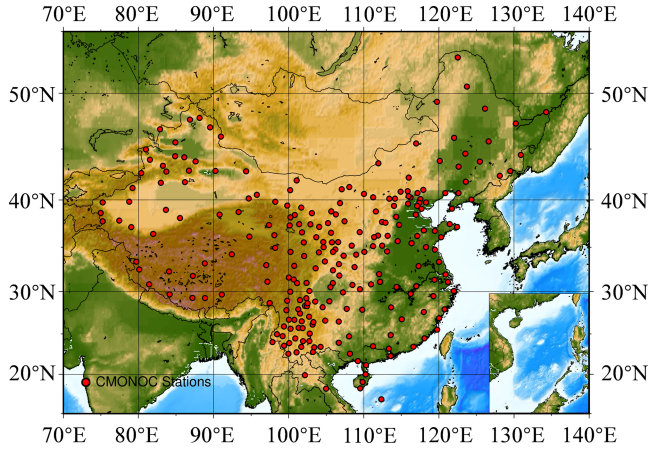

Fig. 1. Geographic locations of GNSS receivers from CMONOC.

III. Construction of Ionospheric TEC Map Prediction Model Using ConvGRU Over China

A. Data Preparation

To some extent, geomagnetic activity and solar activity can reflect the variation trend of ionospheric TEC. In this article, the commonly used geomagnetic activity indices ap, Kp, Dst, and solar activity index F10.7 are selected as the input features of the models when constructing the input datasets of the ConvLSTM model and ConvGRU model. The GNSS observations from 250 CMONOC stations are used to establish the regional ionospheric maps (RIMs) of China (CRIMs) based on the spherical harmonic function model. Then, we use the deep learning method and the CRIMs as the training set to predict the ionospheric TEC. The longitude of the experimental region is from 70°E to 140°E, and the latitude of the experimental region is from 15°N to 55°N. The intervals in the longitude and latitude directions are 1°. Fig. 1 shows the locations of GNSS receivers from CMONOC.

The CRIMs from 2015 to 2018 are selected for the experiment. We select 90% of the ionospheric TEC from 2015 to 2017 as the training set of the model to train the model, 10% of the ionospheric TEC as the verification set to adjust the hyperparameters of the model, and the TEC of 2018 as the model test set to verify the prediction accuracy of the model. In addition, we add the geomagnetic indices which are ap, Kp, and Dst, and the solar activity index which is F10.7 as the training set to analyze the forecasting precision of the model (using -A if there are no indices and -B if there are indices). The sample inputs of the two types of models are 12 TEC maps of a day and the corresponding feature vectors, which can be expressed as a 5-D tensor of (N, 12, 41, 71, C). The sample output is a 5-D tensor of (N, 12, 41, 71, 1), where N denotes the total number of RIMs, 41 and 71 correspond to the dimensions of a TEC map, and C denotes the number of input or output features, with dimension 1 when the sample contains only TEC data, and dimension 5 when geomagnetic activity and solar activity indices are added.

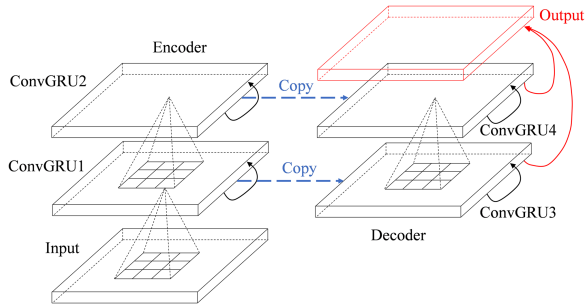

Fig. 2. Encoder–decoder ConvGRU network for forecasting.

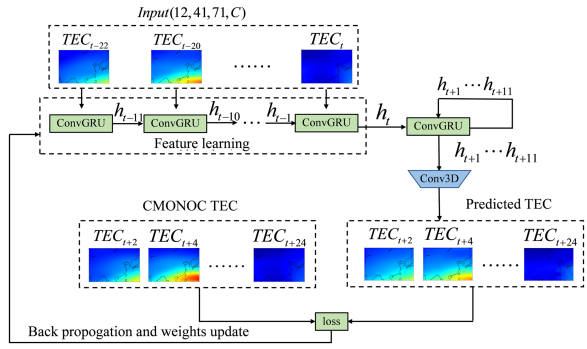

Fig. 3. Flowchart of prediction based on ConvGRU model.

B. Construction of ConvGRU Prediction Model

The ConvGRU structure shown in Fig. 2 is used to establish a regional TEC prediction model in China, which consists of an encoding network and a decoding network. The initial state and cell outputs of the decoding network are copied from the last state of the encoding network [31]. The feature extraction capability of the network can be enhanced by stacking ConvGRU layers, which will improve the prediction capability of the model for spatio-temporal sequence problems. Since the forecast results of the model have the same dimensionality as the input, the final forecast results can be generated by serially decoding all the hidden states in the network and passing them through the 3-D convolution layer. If the input is multichannel, 3-D convolution can also transform the multichannel output into a single-channel output.

As shown in Fig. 3, we demonstrate the overall process of China's regional TEC forecast constructed by the ConvGRU model. During model training, 12 CRIMs of one day are selected each time as the model input to the decoding network. The hidden state at the last moment is obtained by learning the correlation and image features between TEC maps at adjacent moments. It includes the feature information of all 12 images and the timing information. Then, the decoding network is processed and the forecast TEC map for the next day is obtained by cycling the output 12 times. A loss calculation, which is computed during the training process for backpropagation, is performed to compare the forecast results with the true values, and the network parameters are updated using an optimizer so that the model outputs a forecast that continuously approximates the true values.

TABLE I
MODEL TIME COMPLEXITY AND SPACE COMPLEXITY (PER LAYER)

Model	Time complexity	Spatial complexity
DCGAN	2*O(n*k*h*w)	2*O(n*k*h*w)
BP	O (n*d*d)	O (d*d)
LSTM	O (n*d*d)	O (n*d)
CNN-LSTM	O (n*k*h*w+n*d*d)	O (n*h*w*c+n*d)
ConvLSTM	O (n*k* k*h*w)	O (n*h*w*c)
GRU	O (n*d*d)	O (n*d)
ConvGRU	O (n*k*h*w)	O (n*h*w*c)

Note: The table presents the variables used in the model: n for the input batch size, d for the hidden layer dimension, k for the convolution kernel size, h and w for the feature map's width and height, and c for the number of channels.

In this article, the final prediction model consists of four layers of ConvGRU, and a regularization layer is added after each layer of ConvGRU to increase the stability of the network. Finally, a Conv3D layer is added to convert the output forecast image into a single-channel output. The size of convolution kernels in each ConvGRU layer is 3 × 3. The stacking of multiple layers of a small convolutional kernel can reduce model parameters and have the same sensitivity field as that of a large convolutional kernel. In addition, it can also enhance the nonlinear expression ability of the network. We determine the number of convolutional kernels per layer by selecting several common numbers of convolutional kernels and using the grid search method. The specific steps are to build the model using different combinations of the number of convolutional kernels to carry out, solve for the root mean square error (RMSE) of the verification set, and take the average of the five errors as the final error of the number of convolutional kernels in the group. A set of convolution kernels with the smallest final error is selected to build a TEC forecasting model. Essentially, the prediction of TEC is a regression problem, so "MSE" is chosen as the loss function of the model. Selecting "Adam" for the optimizer adapts the learning rate of the model as it is trained so that the optimal solution is found faster. The maximum number of iterations is set to 400, and when the loss of the validation set has not decreased after 50 consecutive iterations, the iteration ends early. The grid search method determines that the number of convolution kernels of each ConvGRU layer in the final ConvGRU model network structure is 40. The parameters setting of the ConvLSTM model is the same as the ConvGRU model to carry out the comparative experiments. After constructing the model, we counted the number of hyperparameters for both models. The total parameters of the ConvLSTM model are 412 761 and the ConvGRU model are 309 841. We can find that ConvGRU has a smaller number of parameters that require less computing power.

IV. EXPERIMENTS AND DISCUSSION

Table I shows the time and space complexity of different models in this article. Time and space complexity are commonly used in algorithmic research to compare factors such as model training time and memory usage. Generally, higher

TABLE II
CLASSIFICATION OF GEOMAGNETIC STORMS

Storm class	Kp	ap (nT)	Dst (nT)
quiet	0<Kp≤4	0<ap≤32	-30<Dst
weak	4<Kp≤5	32< ap≤60	-50< Dst≤-30
moderate	5<Kp≤6	60< ap≤100	-100< Dst≤-50
strong	6<Kp≤7	100< ap≤200	-200< Dst≤-100
severe	7<Kp	200< ap	-300< Dst≤-200

TABLE III
CLASSIFICATION OF SOLAR ACTICITY

Solar activity levels	F10.7 (sfu)
low	0<F10.7⩽100
medium	100<F10.7⩽150
high	150<F10.7

time complexity means longer training time and higher space complexity means more memory usage during training. Table I shows that the DCGAN method has twice the time and space complexity of ConvGRU. The time and space complexity of the BP neural network are greatly influenced by the dimensionality of the hidden layer, which is the second power of the dimension of the hidden layer. Given the dimensionality of the input data required for forecasting regional ionospheric TEC, both time and space complexity are high. Although LSTM outperforms BP neural networks in terms of spatial complexity, the fully connected layers in LSTM still significantly increase the time and spatial complexity of the model. The CNN-LSTM model, which loosely couples CNN and LSTM, has a time and spatial complexity that is the sum of CNN and LSTM, with LSTM still in the form of fully connected layers. The GRU model is similar to the CNN-LSTM model but with fewer gating units. However, the fully connected form still results in higher time and space complexity compared to ConvGRU. Compared to previous models, the ConvLSTM model outperforms in terms of time and space complexity. Although its space complexity is not as high as the previous models, it still achieves significantly better performance. However, it is equal to the ConvGRU model in terms of space complexity, but its time complexity is still higher than that of ConvGRU due to one more gate unit and one more memory cell within ConvLSTM than ConvGRU. In summary, ConvGRU performed well on both evaluation metrics, excelling in terms of training duration and memory usage.

Many studies have shown that ionospheric TEC responds to geomagnetic activity and solar activity. The forecasting precision of TEC on geomagnetic storm days or high solar activity years is lower than that on geomagnetic quiet days or low solar activity years. To a certain extent, the forecasting precision of the forecast model for the TEC of the magnetic storm day can reflect the reliability of the forecast model. Fig. 4 illustrates the geomagnetic activity indices and solar activity index from day of year (DOY) 231–240 in 2018. Fig. 4(a) shows the ap and F10.7 index, and Fig. 4(b) shows the Dst and Kp index. Tables II and III show the classification of magnetic storms and solar activity [32], [33], [34], respectively. To classify the intensities

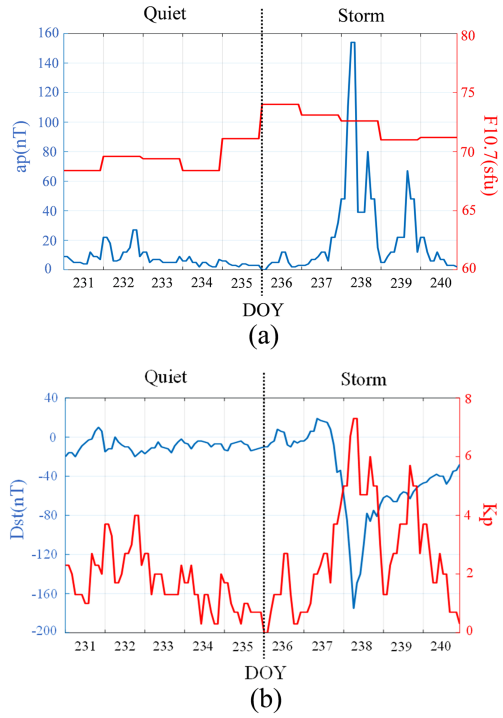

Fig. 4. Variations of geomagnetic and solar activity index (DOY 231–240). (a) Ap index and F10.7 index. (b) Dst index and Kp index.

of storms, the minimum Dst index is used as a criterion. A day is classified as a geomagnetic storm day if the Dst index is less than −30 nT according to the criterion in Table II. There are 202 days of weak storms, 105 days of moderate storms, 16 days of strong storms, and 3 days of severe storms in the training set. In Fig. 4, geomagnetic indices ap, Kp, Dst, and solar flux index F10.7 are used to check the variation of ionosphere from DOY 231–240 in 2018. According to Tables II and III, it can be seen that the Dst index of DOY 231–235 is greater than -30 nT, the ap index is less than 32 nT, and the Kp index is less than 4. Therefore, DOY 231–235 is geomagnetic quiet day. During DOY 236–240, the maximum value of ap and Kp index is 154 nT and 7.3 in DOY 238, respectively. The minimum value of Dst index is -175 nT. Therefore, a large magnetic storm occurs in DOY 236–240. During DOY 231–240, the F10.7 index is all less than 75 sfu. Therefore, solar activity is weak during DOY 231–240, which has little influence on the ionospheric TEC. In this article, DOY 231–235 and DOY 236–240 are selected to analyze the prediction accuracy of geomagnetic quiet and storm time, respectively.

In this study, we use the RMSE, mean absolute error (MAE), and correlation to assess the performance of these models. These functions can be written as

$$\begin{cases} \mathrm{MAE}_{\mathrm{loc}} = \frac{1}{T}\sum_{t=1}^{T}\left|\mathrm{TEC}_{\mathrm{loc}}^{\mathrm{real}}(t) - \mathrm{TEC}_{\mathrm{loc}}^{\mathrm{pred}}(t)\right| \\ \mathrm{RMSE}_{\mathrm{loc}} = \sqrt{\frac{1}{T}\sum_{t=1}^{T}\left(\mathrm{TEC}_{\mathrm{loc}}^{\mathrm{real}}(t) - \mathrm{TEC}_{\mathrm{loc}}^{\mathrm{pred}}(t)\right)^2} \\ \mathrm{RMSE} = \frac{1}{N_{\mathrm{loc}}}\sum_{\mathrm{loc}=1}^{N_{\mathrm{loc}}}\mathrm{RMSE}_{\mathrm{loc}} \\ \mathrm{MAE} = \frac{1}{N_{\mathrm{loc}}}\sum_{\mathrm{loc}=1}^{N_{\mathrm{loc}}}\mathrm{MAE}_{\mathrm{loc}} \\ \rho = \frac{1}{T}\sum_{t=1}^{T}\frac{\mathrm{cov}(\mathrm{TEC}^{\mathrm{real}}(t),\mathrm{TEC}^{\mathrm{pred}}(t))}{\sigma_{\mathrm{TEC}^{\mathrm{real}}(t)}\cdot\sigma_{\mathrm{TEC}^{\mathrm{pred}}(t)}} \end{cases} \tag{3}$$

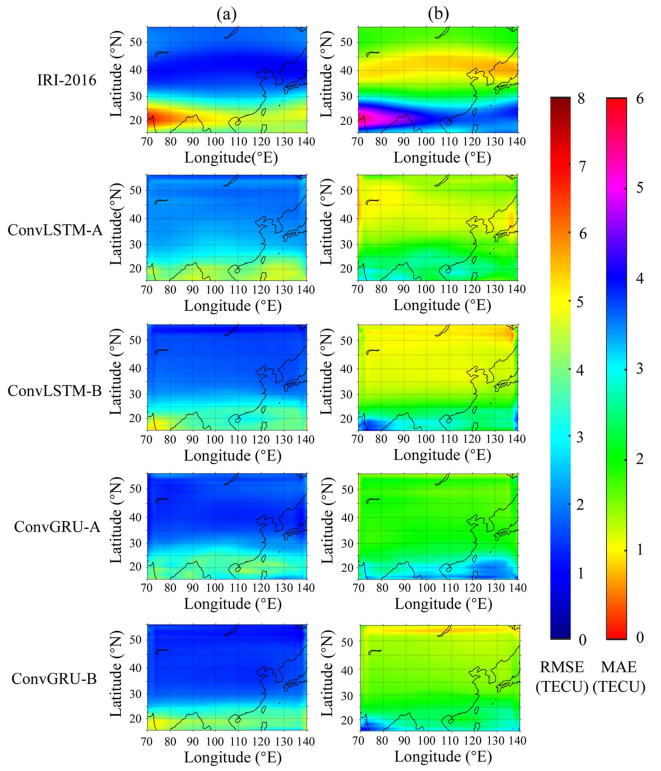

Fig. 5. RMSE and MAE of different models during the geomagnetic quiet time. (a) RMSE (left column). (b) MAE (right column).

where T represents the sample size, loc corresponds to a grid point in China, and $N_{\text{loc}} = 41 \times 71 = 2911$. $\text{TEC}_{\text{loc}}^{\text{real}}(t)$ and $\text{TEC}_{\text{loc}}^{\text{pred}}(t)$ represent the CRIM TEC and the TEC forecast values by different models, respectively, at the time t. $\text{TEC}^{\text{real}}(t)$ and $\text{TEC}^{\text{pred}}(t)$ represent the CRIM TEC sequence and the sequence of TEC prediction values of all the grid points at time t. ρ is the correlation coefficient. $\text{cov}(\text{TEC}^{\text{real}}(t), \text{TEC}^{\text{pred}}(t))$ is the covariance between $\text{TEC}^{\text{real}}(t)$ and $\text{TEC}^{\text{pred}}(t)$. $\sigma_{\text{TEC}^{\text{real}}(t)}$ and $\cdot\sigma_{\text{TEC}^{\text{pred}}(t)}$ are the standard deviations of $\text{TEC}^{\text{real}}(t)$ and $\text{TEC}^{\text{pred}}(t)$, respectively.

A. Geomagnetic Quiet Period

To assess the prediction accuracy of different models during geomagnetic quiet time, RMSE (left column) and MAE (right column) of TEC forecast values of the IRI-2016, ConvLSTM-A, ConvGRU-A, ConvLSTM-B, and ConvGRU-B models are shown in Fig. 5 during DOY 231–235. Table IV shows the average RMSE, MAE, and correlation coefficient of the five models during DOY 231–235. Fig. 5 and Table IV show that the RMSE and MAE of the five models all give a decreasing trend with increasing latitude, and the change of RMSE in the longitude direction is not obvious. After the ConvLSTM and ConvGRU models are added to these indices, the forecasting precision of the model is improved. The RMSE is reduced by 12.8% and 2.7%, respectively. MAE is reduced by 17.2% and 3.6%, respectively. ρ of ConvLSTM-B model is reduced by 0.014 compared to the ConvLSTM-A model, and ρ of ConvGRU-B model is improved by 0.012 compared to the ConvGRU-A model. In addition, compared with the IRI model and ConvLSTM model, the RMSE of ConvGRU-B is reduced by 19% and 7.8%, the MAE is reduced by 27.5% and 9.6%, and ρ is increased by 0.37 and 0.035, respectively. It can be seen that the deep learning models outperform the IRI-2016 model in predicting magnetically quiet days, regardless of whether the geomagnetic and solar activity indices are introduced into the ConvLSTM and ConvGRU models. ρ is significantly higher than the IRI-2016 model. The performance of the ConvGRU-B model is better than that of the other four models, but the performance of the ConvGRU-A model is not significantly improved on magnetic quiet days.

TABLE IV
COMPARISON OF PREDICTION ERRORS BY DIFFERENT MODELS DURING THE GEOMAGNETIC QUIET TIME

Forecast model	Evaluation index		
	RMSE(TECU)	MAE(TECU)	ρ
IRI-2016	2.63	2.22	0.587
ConvLSTM-A	2.65	2.15	0.936
ConvLSTM-B	2.31	1.78	0.922
ConvGRU-A	2.19	1.67	0.945
ConvGRU-B	2.13	1.61	0.957

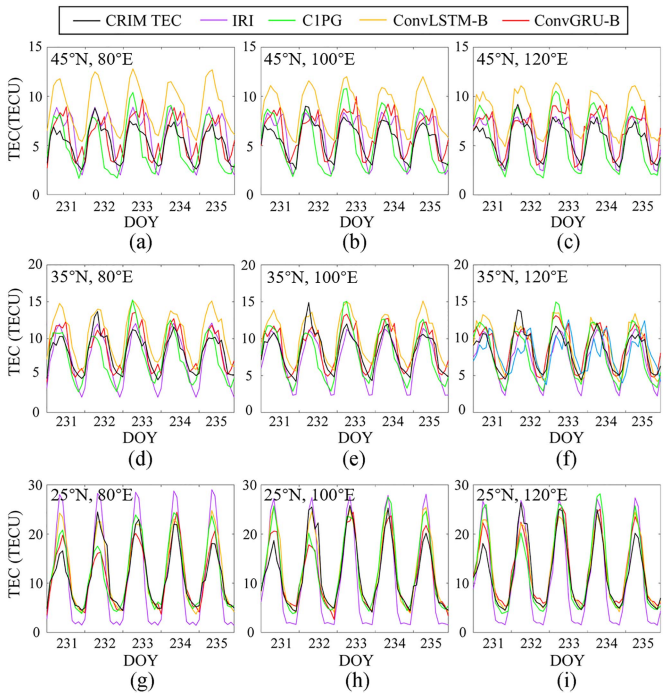

Fig. 6. CRIM TEC and predicted TEC by different models of different grid points during the geomagnetic quiet time.

Also, we use the CODE's 1-day predicted Global Ionospheric Map (C1PG) released by the CODE to assess the performance of the models. Fig. 6 illustrates the CRIM TEC and the 5-day predicted TEC of the other four models in China during geomagnetic quiet time. Table V shows the average RMSE of the 5-day predicted TEC of the four models. From Fig. 6 and Table V, it can be seen that the predicted TEC of the ConvGRU-B model is

TABLE V
AVERAGE RMSE OF DIFFERENT GRID POINTS IN THE EXPERIMENTAL AREA DURING THE GEOMAGNETIC QUIET TIME

Latitude	Longitude		
	80°E	100°E	120°E
45°N	1.45/3.83/1.7 /**1.4**	**1.15**/3.18/1.65/ 1.4	**1.11**/2.78/1.58/ 1.43
35°N	1.54/2.75/1.9 6/**1.5**	1.61/2.26/1.89/ **1.45**	1.64/1.99/1.78/ **1.41**
25°N	5.01/2.71/3.0 2/**2.46**	4.13/2.66/3.17/ **2.64**	3.9/2.38/3.29/**2. 3**

Note : "·/·/·/·" represents the RMSE of the IRI-2016 /C1PG/ConvLSTM-B/ConvGRU-B model

The bold indicates It is intended to distinguish the best forecasts from other comparisons.

TABLE VI
COMPARISON OF PREDICTION ERRORS BY DIFFERENT MODELS DURING THE GEOMAGNETIC STORM TIME

Forecast model	Evaluation index		
	RMSE(TECU)	MAE(TECU)	ρ
IRI-2016	3.31	2.69	0.573
ConvLSTM-A	3.71	2.85	0.925
ConvLSTM-B	2.73	1.94	0.918
ConvGRU-A	3.57	2.33	0.945
ConvGRU-B	2.57	1.82	0.932

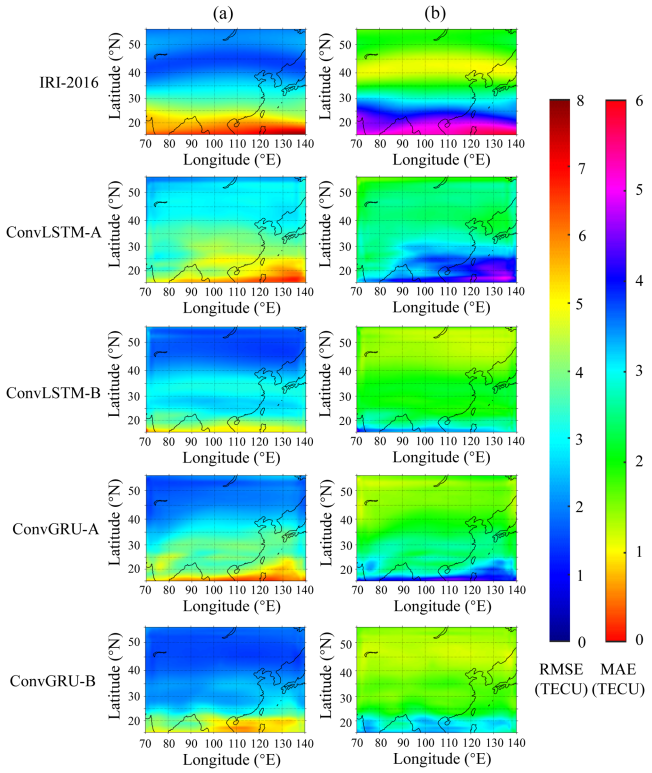

Fig. 7. RMSE and MAE of different models during the geomagnetic storm time. (a) RMSE (left column). (b) MAE (right column).

closer to CRIM TEC. The predicted TEC of IRI-2016 at 25°N and 35°N significantly deviates from CRIM TEC, but the RMSE is the smallest among the four models at (45°N, 100°E) and (45°N, 120°E). The RMSE of ConvGRU-B is lower than that of the other three models. The RMSE of C1PG is higher than that of the other three models at 45°N. The average RMSE of these grid points of IRI-2016, C1PG, ConvLSTM-B, and ConvGRU-B models is 2.39 TECU, 2.73 TECU, 2.28 TECU, and 1.84 TECU, respectively. Compared with IRI-2016, C1PG, and ConvLSTM-B models, the RMSE of the ConvGRU-B model is decreased by 23%, 32.6%, and 19.3%, respectively. The prediction accuracy of the ConvGRU-B model is the highest among the four models when the TEC of these grid points is predicted during geomagnetic quiet time.

B. Geomagnetic Storm Period

Fig. 7 shows the RMSE (left column) and MAE (right column) of predicted TEC of the five models during DOY 236–240. Table VI shows the average RMSE, MAE, and ρ. It can be seen that the RMSE and MAE of the five models also show a downward trend with the latitude change on the magnetic storm day, and the variation in the longitude direction is not obvious. This is consistent with the variation characteristics of magnetic quiet days. RMSE_{loc} and MAE_{loc} of the IRI-2016 model are significantly higher than those of the other four models in the low-latitude region. The maximum RMSE_{loc} of IRI-2016, ConvLSTM-A, ConvLSTM-B, ConvGRU-A, and ConvGRU-B are 7.94 TECU, 6.82 TECU, 6.95 TECU, 7.14 TECU, and 5.98 TECU during geomagnetic storm time, respectively. The maximum MAE_{loc} of the ConvGRU-B model is 5.83 TECU, 5.03 TECU, 4.73 TECU, 4.07 TECU, and 3.7 TECU, respectively. The maximum RMSE_{loc} and MAE_{loc} of the ConvGRU-B model is significantly lower than those of the other four models. Also, it can be found that RMSE_{loc} and MAE_{loc} of low latitude regions can be significantly improved by adding the geomagnetic and solar activity index in the models. In Table VI, the RMSE and MAE of ConvLSTM-B are decreased by 26.4% and 31.9% compared with ConvLSTM-A, respectively. RMSE and MAE of ConvGRU-B decreased by 28% and 21.9% compared with ConvGRU-A, respectively. ρ of the other four models is higher than that of the IRI-2016 model, and ρ of ConvGRU model is obviously higher than that of the ConvLSTM model. The RMSE and MAE of ConvGRU-B are 22.4% and 32.3% lower than those of the IRI-2016 model, and 5.9% and 6.2% lower than those of ConvLSTM-B, respectively. In short, the addition of geomagnetic activity and solar activity index can effectively improve the prediction accuracy of geomagnetic storm time. The forecast precision of ConvGRU-B is higher than that of the other four models.

We also use the predicted TEC and CRIM TEC to do the accuracy assessment. Fig. 8 shows CRIM and predicted TEC by different models of different grid points during the geomagnetic storm time. Table VII shows the average RMSE of predicted TEC by four models during DOY 236–240. In Fig. 8 and Table VII, RMSE of all four models decreases with increasing latitude, and the variation with longitude is not obvious. The predicted TEC values of the three grid points of the IRI-2016 model at 25°N deviate significantly from the

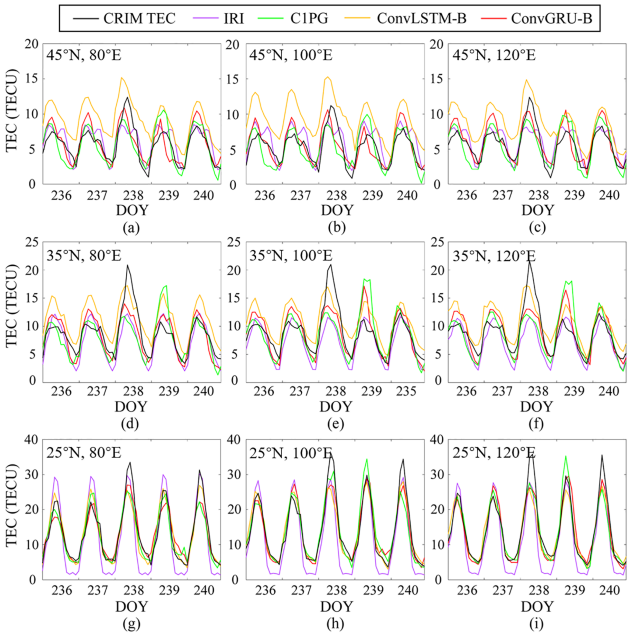

Fig. 8. CRIM-TEC and predicted TEC by different models of different grid points during the geomagnetic storm time.

TABLE VII
AVERAGE RMSE OF DIFFERENT GRID POINTS IN THE EXPERIMENTAL AREA DURING THE GEOMAGNETIC STORM TIME

Latitude	Longitude		
	80°E	100°E	120°E
45°N	1.63/4.4/1.8/**1.58**	**1.5**/3.73/1.74/1.54	1.46/3.24/1.53/**1.46**
35°N	2.61/3.25/3.03/**2.2**	2.82/2.78/3.13/**2.37**	2.81/2.49/3.14/**2.4**
25°N	4.57/2.74/3.06/**2.73**	4.42/2.8/3.07/**2.73**	4.4/3.08/3.03/**2.79**

Note: "·/·/·/·" represents the RMSE of the IRI-2016 /C1PG/ConvLSTM-B/ConvGRU-B model
The bold indicates It is intended to distinguish the best forecasts from other comparisons.

CRIM TEC. The TEC prediction value of the C1PG model at 45°N deviates significantly from the CRIM TEC. Due to the strong geomagnetic activity on DOY 238, the CRIM TEC of this day is obviously higher than that of the other four days. During a magnetic storm day, the average RMSE of the IRI-2016, C1PG, ConvLSTM-B, and ConvGRU-B models at these grid points are 2.91 TECU, 3.17 TECU, 2.61 TECU, and 2.2 TECU, respectively. Compared with the IRI-2016, C1PG, and ConvLSTM-B models, the RMSE of the ConvGRU-B model is reduced by 24.4%, 30.6%, and 15.7%, respectively. In general, the RMSE of ConvGRU-B at these grid points is smaller than that of the other four models, and the overall prediction accuracy is significantly improved over the IRI-2016 model and C1PG model. In addition, compared with the ConvLSTM-B model, it has also been improved to a certain extent.

C. Prediction Accuracy of TEC in Different Seasons

In this section, we further verify the performance of the ConvGRU model on the ionospheric TEC in different seasons

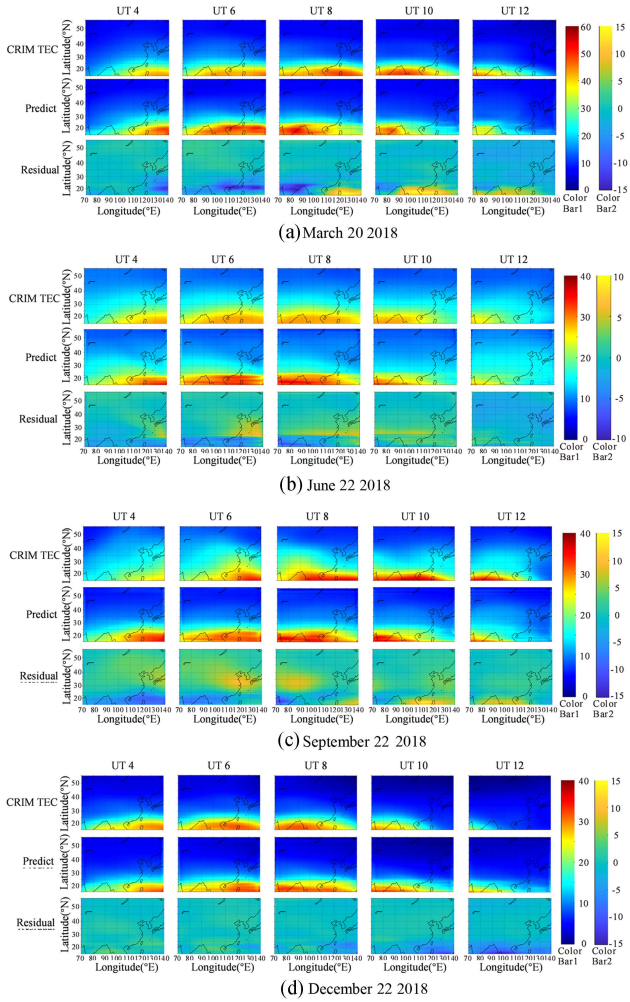

Fig. 9. Predicted value, true value, and corresponding residual value at 4:00 UT, 6:00 UT, 8:00 UT, 10:00 UT, and 12:00 UT on different days (the CRIM and prediction's color scale is based on color bar1, and the residual's color scale is based on color bar2). (a) Spring equinox (March 21st, 2018). (b) Summer solstice (June 20th, 2018). (c) Autumnal equinox (September 23rd, 2018). (d) Winter solstice (December 22nd, 2018).

in China and analyze the influence of the equatorial ionospheric anomaly (EIA) on the forecast precision of the model. Fig. 9 shows the TEC diagrams from UT 4 to UT 12 on March 21, June 22, September 22, and December 22, 2018. It includes the time period from the appearance to the disappearance of EIA in China. The first row of Fig. 9(a)–(d) represents the CRIM TEC, the second row is the predicted TEC of the ConvGRU-B model, and the third row is the residual between CRIM TEC and predicted TEC. The calculation formula can be written as $\mathrm{Residual} = \mathrm{TEC}_t - \mathrm{TEC}_p$, where TEC_t represents the CRIM TEC and TEC_p represents the predicted TEC. Table VIII shows the RMSE, MAE, and ρ of ConvLSTM-B and ConvGRU-B models in these days. It shows that EIA appears in the eastern part of China at UT 4 and moves westward over time, and gradually disappears at UT 12. The maximum CRIM TEC of the spring equinox, summer solstice, autumnal equinox, and winter solstice are 48.7 TECU, 28.9 TECU, 38.1 TECU, and 31.7 TECU, respectively. This indicates that the maximum TEC at the spring

TABLE VIII
COMPARISON OF PREDICTION ERRORS BY THE TWO MODELS ON DIFFERENT DAYS

Date	Forecast model	Evaluation index		
		MAE (TECU)	RMSE (TECU)	ρ
spring equinox (3.21)	ConvLSTM-B	1.95	2.59	0.895
	ConvGRU-B	1.58	2.16	0.925
summer solstice (6.22)	ConvLSTM-B	1.8	2.19	0.869
	ConvGRU-B	1.4	1.8	0.896
autumnal equinox (9.22)	ConvLSTM-B	2.78	3.39	0.568
	ConvGRU-B	2.17	2.72	0.832
winter solstice (12.22)	ConvLSTM-B	1.63	1.91	0.746
	ConvGRU-B	1.26	1.62	0.718

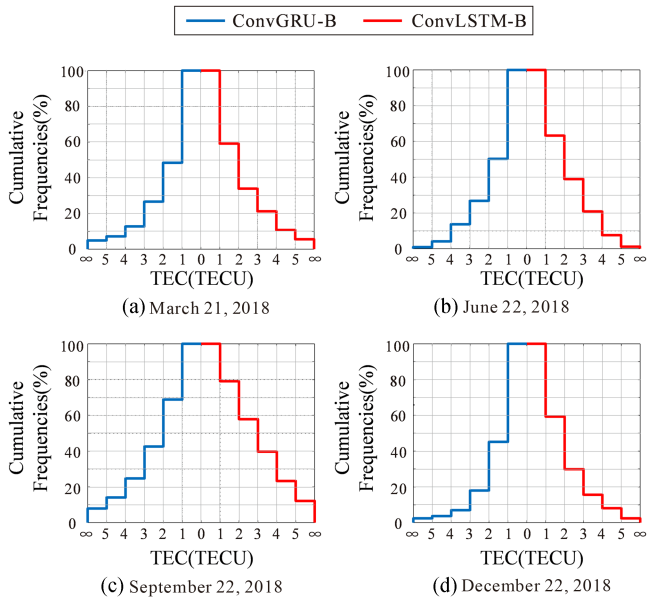

Fig. 10. Cumulative frequencies of MAE of the two models on different days. (a) Spring equinox (March 21st, 2018). (b) Summer solstice (June 20th, 2018). (c) Autumnal equinox (September 23rd, 2018). (d) Winter solstice (December 22nd, 2018).

and autumn equinoxes is higher than that at the summer and winter solstices, which is consistent with the "semi-annual anomaly" phenomenon of the ionosphere. Comparing the predicted results of the ConvGRU-B model with the CRIM TEC value, it can be found that the ConvGRU-B model roughly captures the change of EIA over time, and the area with large residuals basically coincides with the position of EIA. The background TEC of the spring equinox and autumnal equinox are higher than that of the summer solstice and winter solstice leading to the residual of the spring equinox and autumnal equinox higher than that of the summer solstice and winter solstice. Furthermore, the Dst index is less than -30 nT on September 22. A weak geomagnetic storm occurs, which causes the fitting effect of the autumnal equinox to be worse than that of the spring equinox. Fig. 10 shows the MAE accumulated frequency of ConvLSTM-B and ConvGRU-B models throughout the whole day of the different seasons. Table VIII gives the RMSE, MAE, and the two models during the whole day. In Fig. 10 and Table VIII, it can be seen that

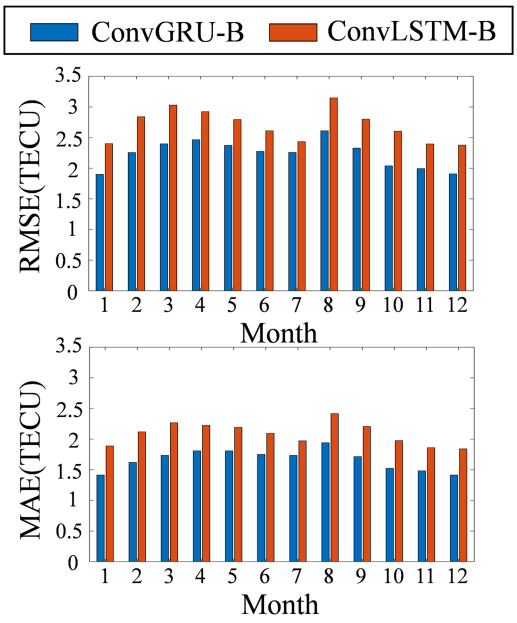

Fig. 11. RMSE and MAE of the two models in different months of 2018.

the percentage of the MAE of the ConvLSTM-B model within the range of 0–1 TECU is 41%, 36.7%, 20.9%, and 40.7%, respectively. The percentage of the MAE of the ConvGRU-B model in the range of 0–1TECU is 51.6%, 49.6%, 31.1%, and 54.8%, respectively. The cumulative MAE frequency distribution of the ConvGRU-B model is obviously better than that of the ConvLSTM-B model. As can be seen from Table VIII, the MAE and RMSE of the ConvGRU-B model are smaller than that of the ConvLSTM-B model, and the error of the autumnal equinox is significantly higher than that of the other three seasons. The error of the ConvGRU-B model is smaller than that of the ConvLSTM-B model except for winter solstice. Based on the previous analysis, the performance of the ConvGRU-B model is also better than that of the ConvLSTM-B model in different seasons.

D. Prediction Accuracy for the Whole Year 2018

Fig. 11 shows the comparison of the RMSE and MAE of the TEC predicted results of the ConvLSTM-B and ConvGRU-B models in 12 months in 2018. The RMSE and MAE of the ConvGRU-B model are smaller than those of the ConvLSTM-B model every month in 2018. Due to the geomagnetic storms, the maximum RMSE and MAE of both models appear in August. The RMSE and MAE of the ConvGRU-B model decrease by 0.63 TECU and 0.53 TECU at most compared to the ConvLSTM-B model. The average RMSE and MAE of the ConvLSTM-B model for 2018 are 2.69 TECU and 2.09 TECU, respectively. The RMSE and MAE of the ConvGRU-B model are 2.24 TECU and 1.66 TECU, which are 16.7% and 20.6% lower than those of the ConvLSTM-B model, respectively. According to the above data, the performance of the ConvGRU-B model is obviously better than that of the ConvLSTM-B model. It has strong forecast stability.

TABLE IX
RMSE(TECU) OF CONVLSTM-B MODEL AND CONVGRU-B MODEL UNDER DIFFERENT GEOMAGNETIC ENVIRONMENTS

Model	Storm class			
	Quiet	Weak	Moderate	Strong
ConvLSTM-B	2.57	2.96	3.56	4.65
ConvGRU-B	2.12	2.34	2.49	3.17

To further analyze the accuracy of the model proposed in this article for TEC forecasting under different geomagnetic conditions in 2018, a total of 41 days are classified as geomagnetic storm days in 2018 according to the criteria in Table II, of which contain 34 days of weak storms, 6 days of moderate storms, and 1 day of large storm, leaving 324 days of geomagnetic quiet days. Magnetic storm days account for 11.2% of the year. Table IX shows the RMSE of the ConvLSTM-B model and the ConvGRU-B model under different geomagnetic environments. The RMSE of the ConvGRU-B model decreased by 17.5%, 20.9%, 30.1%, and 31.8% during geomagnetic quiet days, weak storm days, moderate storm days, and strong storm days compared to that of the ConvLSTM-B model, respectively. It can be seen that the forecast accuracy of the ConvGRU-B model is improved compared with that of the ConvLSTM-B model under different geomagnetic conditions.

V. CONCLUSION

In this article, we develop a ConvGRU deep learning method to construct a short-term forecast model for the ionospheric TEC in China based on geomagnetic indices, solar activity index, and GNSS observation data from CMONOC. The results demonstrate that the prediction accuracy of ConvLSTM-B and ConvGRU-B models is improved on geomagnetic storms, quiet days, and different seasons. The average RMSE and MAE of the ConvGRU-B model are lower than those of the ConvLSTM-B model each month, with the RMSE decreasing by up to 0.63 TECU in a single month and MAE decreasing by 0.53 TECU at most. The annual average RMSE and MAE of the ConvGRU-B model are 2.24 TECU and 1.66 TECU, respectively. Compared to the ConvLSTM-B model, they are decreased by 16.7% and 20.6%, respectively. Furthermore, the RMSE of the ConvGRU-B model decreased by 17.5%, 20.9%, 30.1%, and 31.8% during geomagnetic quiet days, weak storm days, moderate storm days, and strong storm days compared to that of the ConvLSTM-B model respectively. In general, the ConvGRU-B model proposed has higher prediction accuracy than the ConvLSTM-B model and is better than the IRI-2016 and C1PG models. In the future, we will further modify the structure of the ConvGRU unit affected by the physical patterns of the ionosphere to enhance the performance of the model in capturing spatio-temporal features.

ACKNOWLEDGMENT

The authors would like to thank the CMONOC for providing the GPS data via the GNSS Center, Wuhan University and the GIRO for providing the ionosonde data.

REFERENCES

[1] J. A. Klobuchar, "Ionospheric time-delay algorithm for single-frequency GPS users," *IEEE Trans. Aerosp. Electron. Syst.*, vol. AES-23, no. 3, pp. 325–331, May 1987.
[2] Y. Yuan et al., "Refining the Klobuchar ionospheric coefficients based on GPS observations," *IEEE Trans. Aerosp. Electron. Syst.*, vol. 44, no. 4, pp. 1498–1510, Oct. 2008.
[3] D. Bilitza et al., "International Reference Ionosphere 2016: From ionospheric climate to real-time weather predictions," *Space Weather*, vol. 15, no. 2, pp. 418–429, Feb. 2017.
[4] B. Nava, P. Coïsson, and S. M. Radicella, "A new version of the NeQuick ionosphere electron density model," *J. Atmos. Sol.-Terr. Phys.*, vol. 70, no. 15, pp. 1856–1862, Dec. 2008.
[5] Y. Yuan, N. Wang, Z. Li, and X. Huo, "The BeiDou global broadcast ionospheric delay correction model (BDGIM) and its preliminary performance evaluation result," *Navigation*, vol. 66, no. 1, pp. 55–69, Jan. 2019.
[6] J. Tang, Y. Li, D. Yang, and M. Ding, "An approach for predicting global ionospheric TEC using machine learning," *Remote Sens.*, vol. 14, no. 7, Mar. 2022, Art. no. 1585.
[7] A. García-Rigo et al., "Global prediction of the vertical total electron content of the ionosphere based on GPS data," *Radio Sci.*, vol. 46, no. 6, Dec. 2011, Art. no. RS0D25.
[8] D. Roma-Dollase et al., "Consistency of seven different GNSS global ionospheric mapping techniques during one solar cycle," *J. Geodesy*, vol. 92, no. 6, pp. 691–706, Jun. 2017.
[9] Z. Huang, Q. B. Li, and H. Yuan, "Forecasting of ionospheric vertical TEC 1-h ahead using a genetic algorithm and neural network," *Adv. Space Res.*, vol. 55, no. 7, pp. 1775–1783, Apr. 2015.
[10] R. Song, X. Zhang, C. Zhou, J. Liu, and J. He, "Predicting TEC in China based on the neural networks optimized by genetic algorithm," *Adv. Space Res.*, vol. 62, no. 4, pp. 745–759, Aug. 2018.
[11] S. Lee, E. Y. Ji, Y. J. Moon, and E. Park, "One-day forecasting of global TEC using a novel deep learning model," *Space Weather*, vol. 19, no. 1, Jan. 2021, Art. no. e2020SW002600.
[12] A. Ruwali, A. J. Sravan Kumar, K. B. Prakash, G. Sivavaraprasad, and D. Venkata Ratnam, "Implementation of hybrid deep learning model (LSTM-CNN) for ionospheric TEC forecasting using GPS data," *IEEE Geosci. Remote Sens. Lett.*, vol. 18, no. 6, pp. 1004–1008, Jun. 2021.
[13] S. Sahu, R. Trivedi, R. K. Choudhary, A. Jain, and S. Jain, "Prediction of total electron content (TEC) using neural network over anomaly crest region Bhopal," *Adv. Space Res.*, vol. 68, no. 7, pp. 2919–2929, Oct. 2021.
[14] P. Xiong, D. Zhai, C. Long, H. Zhou, X. Zhang, and X. Shen, "Long short-term memory neural network for ionospheric total electron content forecasting over China," *Space Weather*, vol. 19, no. 4, Apr. 2021, Art. no. e2020SW002706.
[15] J. Chen, N. Zhi, H. Liao, M. Lu, and S. Feng, "Global forecasting of ionospheric vertical total electron contents via ConvLSTM with spectrum analysis," *GPS Solutions*, vol. 26, no. 3, pp. 69–78, Apr. 2022.
[16] Z. Chen, W. Liao, H. Li, J. Wang, X. Deng, and S. Hong, "Prediction of global ionospheric TEC based on deep learning," *Space Weather*, vol. 20, no. 4, Apr. 2022, Art. no. e2021SW002854.
[17] X. Ren, P. Yang, H. Liu, J. Chen, and W. Liu, "Deep learning for global ionospheric TEC forecasting: Different approaches and validation," *Space Weather*, vol. 20, no. 5, May 2022, Art. no. e2021SW003011.
[18] D. Yang, H. Fang, and Z. Liu, "Completion of global Ionospheric TEC maps using a deep learning approach," *J. Geophys. Res., Space Phys.*, vol. 127, no. 5, May 2022, Art. no. e2022JA030326.
[19] K. Sivakrishna, D. Venkata Ratnam, and G. Sivavaraprasad, "A bidirectional deep-learning algorithm to forecast regional ionospheric TEC maps," *IEEE J. Sel. Topics Appl. Earth Observ. Remote Sens.*, vol. 15, pp. 4531–4543, Jun. 2022.
[20] G. Xia, F. Zhang, C. Wang, and C. Zhou, "ED-ConvLSTM: A novel global ionospheric total electron content medium-term forecast model," *Space Weather*, vol. 20, no. 8, Aug. 2022, Art. no. e2021SW002959.
[21] L. Liu, Y. J. Morton, and Y. Liu, "ML prediction of global ionospheric TEC maps," *Space Weather*, vol. 20, no. 9, Sep. 2022, Art. no. e2022SW003135.
[22] M. Lin, X. Zhu, G. Tu, and X. Chen, "Optimal transformer modeling by space embedding for ionospheric total electron content prediction," *IEEE Trans. Instrum. Meas.*, vol. 71, 2022, Art. no. 8505414.
[23] Y. Liu, J. Wang, C. Yang, Y. Zheng, and H. Fu, "A machine learning-based method for modeling TEC regional temporal-spatial map," *Remote Sens.*, vol. 14, no. 21, Nov. 2022, Art. no. 5579.

[24] X. Gao and Y. Yao, "A storm-time ionospheric TEC model with multi-channel features by the spatiotemporal ConvLSTM network," *J. Geodesy*, vol. 97, no. 1, Jan. 2023, Art. no. 9.
[25] B. Zhang, J. Ou, Y. Yuan, and Z. Li, "Extraction of line-of-sight ionospheric observables from GPS data using precise point positioning," *Sci. China Earth Sci.*, vol. 55, no. 11, pp. 1919–1928, Nov. 2012.
[26] T. Liu, B. Zhang, Y. Yuan, Z. Li, and N. Wang, "Multi-GNSS triple-frequency differential code bias (DCB) determination with precise point positioning (PPP)," *J. Geodesy*, vol. 93, no. 5, pp. 765–784, May 2019.
[27] Y. Xiang and Y. Gao, "Improving DCB estimation using uncombined PPP," *Navigation*, vol. 64, no. 4, pp. 463–473, Oct. 2017.
[28] J. Liu, R. Chen, H. Kuusniemi, Z. Wang, and Y. Jian, "A preliminary study on mapping the regional ionospheric TEC using a spherical cap harmonic model in high latitudes and the arctic region," *J. Glob. Positioning Syst.*, vol. 9, no. 1, pp. 22–32, Jun. 2010.
[29] J. Liu, R. Chen, Z. Wang, and H. Zhang, "Spherical cap harmonic model for mapping and predicting regional TEC," *GPS Solutions*, vol. 15, no. 2, pp. 109–119, Jun. 2011.
[30] Y. Yuan et al., "Monitoring the ionosphere based on the crustal movement observation network of China," *Geodesy Geodyn.*, vol. 6, no. 2, pp. 73–80, Mar. 2015.
[31] X. Shi, Z. Chen, H. Wang, D. Y. Yeung, W. K. Wong, and W. C. Woo, "Convolutional LSTM network: A machine learning approach for precipitation nowcasting," in *Proc. 28th Int. Neural Inf. Process Syst.*, 2015, vol. 1, pp. 802–810.
[32] W. D. Gonzalez et al., "What is a geomagnetic storm?," *J. Geophys. Res., Space Phys.*, vol. 99, no. A4, pp. 5771–5792, Apr. 1994.
[33] C. A. Loewe and G. W. Prölss, "Classification and mean behavior of magnetic storms," *J. Geophys. Res., Space Phys.*, vol. 102, no. A7, pp. 14209–14213, Jan. 1997.
[34] G. Jee, H. B. Lee, Y. H. Kim, J. K. Chung, and J. Cho, "Assessment of GPS global ionosphere maps (GIM) by comparison between CODE GIM and TOPEX/Jason TEC data: Ionospheric perspective," *J. Geophys. Res., Space Phys.*, vol. 115, no. A10, Oct. 2010, Art. no. A10319.

Jun Tang received the B.S. and M.S. degrees in geodesy and surveying engineering from the East China University of Technology, Fuzhou, China, in 2006 and 2009, respectively, and the Ph.D. degree in geodesy and surveying engineering from Wuhan University, Wuhan, China, in 2014.

He is currently a Professor with the Faculty of Land Resources Engineering, Kunming University of Science and Technology, Kunming, China. His research interests include Global Navigation Satellite Systems (GNSS) data processing, ionospheric modeling using GNSS data, and multidimensional ionospheric tomography based on GNSS observations and GNSS applications.

Zhengyu Zhong received the B.S. degree in traffic engineering from Shenzhen University, Shenzhen, China, in 2020, and the M.S. degree in transportation engineering from the School of Transportation Engineering, East China Jiaotong University, Nanchang, China, in 2023.

His research interests include Global Navigation Satellite Systems ionospheric modeling and ionospheric parameter forecasting.

Mingfei Ding received the B.S. degree in computer science and technology from Northeast Agricultural University, Harbin, China, in 2020. He is currently working toward the M.S. degree in geodesy and surveying engineering with the School of Transportation Engineering, East China Jiaotong University, Nanchang, China.

His research interests include Global Navigation Satellite Systems ionospheric modeling and ionospheric parameter forecasting based on deep learning.

Dengpan Yang received the B.S. degree in surveying and mapping engineering from Henan Polytechnic University, Jiaozuo, China, in 2021. She is currently working toward the M.S. degree in geodesy and surveying engineering with the School of Transportation Engineering, East China Jiaotong University, Nanchang, China.

Her research interests include ionospheric parameter prediction and Global Navigation Satellite Systems ionospheric disturbance detection.

Heng Liu received the B.S. degree in communication engineering from Wuhan University of Engineering Science, Wuhan, China, in 2017. He is currently working toward the M.S. degree in geodesy and surveying engineering with the School of Transportation Engineering, East China Jiaotong University, Nanchang, China.

His current research focuses on Global Navigation Satellite Systems ionospheric modeling.